Journal of Alloys and Compounds 585 (2014) 753–759

Contents lists available at ScienceDirect

Journal of Alloys and Compounds

journal homepage: www.elsevier.com/locate/jalcom

The effects of room temperature ECAP and subsequent aging on mechanical properties of 2024 Al alloy

M.H. Goodarzy [a,*], H. Arabi [b], M.A. Boutorabi [b], S.H. Seyedein [a], S.H. Hasani Najafabadi [c]

[a] School of Metallurgy and Materials Engineering, Iran University of Science & Technology (IUST), Narmak, Tehran 13114-16846, Iran
[b] Center of Excellence for High Strength Alloys Technology (CEHSAT), School of Metallurgy and Materials Engineering (IUST), Narmak, Tehran 13114-16846, Iran
[c] Department of Mechanical Engineering, Azad University Saveh Branch (AUSB), Saveh 39187-366, Iran

ARTICLE INFO

Article history:
Received 9 April 2013
Received in revised form 27 September 2013
Accepted 30 September 2013
Available online 14 October 2013

Keywords:
ECAP
2024 Aluminum alloy
Aging
Mechanical properties

ABSTRACT

Mechanical properties of the 2024 aluminum alloy, which was plastically deformed by equal channel angular pressing (ECAP) at room temperature and aged naturally and artificially at 70 °C and 100 °C for different times, were investigated in this research. Many of the short shear bands were observed on the microstructure after one pass of ECAP and led to fragmentation of grains. Hardness and yield stress of the sample aged naturally after deformation were considerably improved due to increase of dislocation density calculated by XRD data analysis and their interaction with solute atoms during ECAP. The ductility and work hardening exponent of the deformed samples were significantly reduced due to formation of shear bands within the microstructure. However aging the samples immediately after sever plastic deformation at 70 °C and 100 °C caused an additional improvement in hardness and yield stress relative to the samples aged naturally after deformation.

1. Introduction

Mechanical properties of metal alloys can be improved by forming processes such as ECAP [1,2]. This process presented by Segal et al. [3] at 1977 has been widely used by many researchers since then [4,5]. Mechanical properties of most age-hardenable aluminum alloys can be improved by this method. It is well known that the most part of improvement in mechanical properties of the fully annealed aluminum alloys is achieved in the first pass of ECAP process [4,6]. For example according to Horita et al. [6] fully annealed Al alloys such as 1100, 6061 and 7075 can obtain 80–90% of their maximum values of their yield stress only after one pass ECAP. Also some reports indicate that a significant improvement in mechanical properties of age hardenable aluminum alloys in solution annealing condition, can be achieved via one pass of warm ECAP and subsequent aging at low temperatures [6–8]. For example according to Kim et al. [8], the yield stress of 2024 aluminum alloy can be improved by 110%, i.e. from 320 MPa to 628 MPa after one pass of warm ECAP and subsequent aging at 100 °C for 20–30 h.

It has been reported [8,9] that increase in the dislocation density during ECAP not only improves material strengthening, but also it can increase the rate of precipitation during aging. So that formation of fine precipitates and further improvement in mechanical properties can be expected. However, dynamic recovery in warm ECAP of age hardenable Al alloys can cause a decrease in dislocation density of the deformed material and consequently dislocation strengthening is decreased [10,11]; one should consider cold ECAP as a substitute for deformation of these material. Recently some published reports show that improvement in mechanical properties can be achieved by one pass of cold ECAP in age hardenable aluminum alloy [12–14] due to elimination of dynamic recovery in this process which cause saturation in subgrain dislocation density, hence optimum mechanical properties are achieved [15]. Moreover from economic point of view, according to Bidulsky [16], using one pass of cold ECAP is beneficial for making aluminum PM parts, as application of this process can control the porosity content.

Deformation of aluminum alloys EN AW 2014 by one pass of cold ECAP after solution annealing and water quenching, resulted to improvement of its yield stress from 157 MPa to 511 MPa due to grain refinement and strain hardening of solid solution according to Kvackaj et al. [12,13]. However, subsequent artificial aging at 100 °C did not considerably affect YS & UTS of the ECAPed alloy. In another study, Danaf [14] reported that the usage of one pass of cold ECAP for commercial Al alloys 1050, 5083, 6082 and 7010 result to domination of low angle grain boundaries within the microstructure of ECAPed alloys. The amount of decrease in grain size in his study was considerable especially in age hardenable alloys 6082 and 7010. In addition hardness and yield strength of the ECAPed alloys were sharply increased due to grain refinement and dislocation strengthening during cold ECAP.

The above mentioned reports basically related to the cold ECAP of some Al alloys at room temperature, does not include 2024 Al

* Corresponding author. Tel./fax: +98 2177459151.
E-mail addresses: mh_goodarzy@iust.ac.ir (M.H. Goodarzy), arabi@iust.ac.ir (H. Arabi), boutorabi@iust.ac.ir (M.A. Boutorabi), seyedein@iust.ac.ir (S.H. Seyedein), najafabadiresearch@gmail.com (S.H. Hasani Najafabadi).

0925-8388/$ - see front matter © 2013 Elsevier B.V. All rights reserved.
http://dx.doi.org/10.1016/j.jallcom.2013.09.202

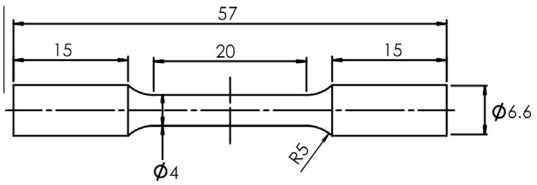

Fig. 1. The shape and dimensions of the sub-sized specimen for tensile test.

alloys which is a high strength age hardenable alloy. About formability, variation of mechanical properties and structural parameters like dislocation density of this alloy by cold ECAP there is no published information. Thus the aim of this study is to investigate the mechanical properties and structural parameter include crystallite domain size, lattice microstrain and dislocation cell size of 2024 Al alloy.

2. Experimental procedure

Commercial aluminum alloy 2024-T8 in the form of extruded rod of 20 mm in diameter with mean chemical composition of Al–4.2Cu–1.26 Mg–0.63Mn–0.42Fe–0.29Si (in wt.%), was used in this research. Cylindrical specimens with a diameter of 11.7 mm and length of 70 mm were made via machining. They were solution annealed at 500 °C for 40 min and quenched in water prior to their deformation. Quenched samples were immediately subjected to severe plastically deformation at room temperature using ECAP die. The die was made from hot work steel (H13). Molybdenum disulfide powder was used as lubricant. The angle between the two channels and the corner die angle were 90° and 22.5° respectively; on the base of Iwahashi Equation [17] an approximate equivalent strain of 1.05 can be applied per pass in the process of ECAP for those angles. Second pass in route B_c [18] was applied immediately after ending the first pass. This pass generated lots of deep cracks in shear direction on the samples and led to failure of the components.

Deformed samples after one pass of ECAP were naturally aged for 72 h. or at 70 °C and 100 °C for various times up to 70 h. to determine the optimum condition of the post-ECAP low temperature aging. Microstructures of longitudinal and transvers sections of the deformed samples after being prepared by conventional metallographic route, i.e. Specimens were mounted, mechanically polished by emery papers from No. 180 to No. 1200 and eventually etched by Keller's reagent (2%Hf + 3%HCl + 5%HNO_3 + 90%H_2O in vol.%), were evaluated by Philips-XL30 scanning electron microscope (SEM) operated at 20 Kv. Elemental analysis of the microstructural features specially inclusions was accomplished by EDAX analyzer.

X-ray diffraction analysis was carried out on the polished sections of the solution annealed and deformed samples in a SEIFERT-3003TT diffractometer using Cu Kα radiation, 40 kV and 30 mA with a scan rate of 0.005°/s. In order to reduce the effect of initial texture on the diffraction peak profiles, XRD peaks were obtained from the longitudinal and cross-sections of the extruded rod and then the average intensities for each sample was considered for construction of a complete diffractogram. In order to remove the error from experimental diffraction of the peaks X-ray profiles due to instrument broadening, FWHM obtained from peak profile of a fully annealed pure aluminum was used for finding structural broadening ΔK_s (i.e. effective FWHM) according to the Stokes method [19]. The average domain size and dislocation density was calculated by the Williamson–Hall [20,21] procedure and the Rietveld method [22] respectively.

Worth mentioning the full-widths at half maximum (FWHM) of experimental diffraction peaks were determined after fitting the scattered X-ray data on pseudo-voigt function. Then by using the Stokes method as given by $\Delta K_s = \Delta K_{exp} - \Delta K_i$ where ΔK_{exp} the experimental FWHM, and ΔK_i the instrumental FWHM, respectively an effective FWHM was obtained for each peak which considered the base of our calculation for finding the average domain size and dislocation density.

Micro-hardness and tensile tests were used to investigate the effect of severe plastic deformation on mechanical properties. Micro-hardness tests were performed under force of 1 Kg for 10 s in cross-sections of the samples and repeated three times for each sample. Tensile tests conducted on the sub-sized sample with dimensions shown in Fig. 1. The gauge length of the samples was 20 mm and their diameter was 4 mm. The test was performed with a strain rate of 1.3×10^{-3} s^{-1} in room temperature using an INSTRON machine.

3. Results and discussion

3.1. Microstructure

The microstructure of the polished specimen of the as-received material after solution annealing is shown in Fig. 2. This microstructure shows there are three types of intermetallic compounds

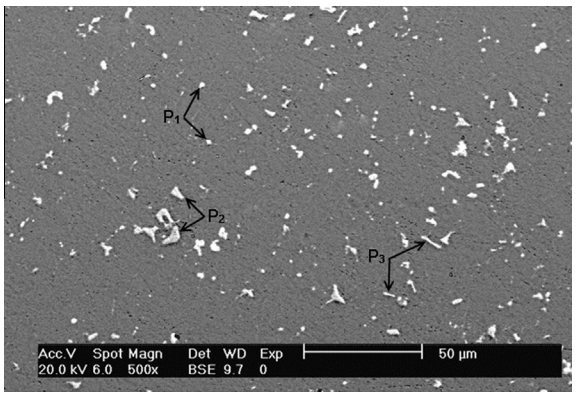

Fig. 2. SEM micrograph of the cross-section of 2024 aluminum alloy rod after solution annealing treatment.

(coded P_1, P_2 and P_3) within the microstructures; the round particles are rich in Al, Cu and Mg, the larger particles having angular shapes are rich in Al, Cu, Fe and Mn and the rod shape particles are rich in Al, Si, Fe, and Mn on the base of the results obtained by EDAX analysis. These results are similar to those obtained by other researches who investigated microstructure of 2024 Al alloy [23,24]. The stoichiometric compositions of these compounds can be given as $CuMgAl_2$ for P_1, $(CuFeMn)Al_6$ for P_2 and $(FeMn)Si_3Al_{17}$ for P_3.

Typical SEM microstructures of the etched samples before and after deformation are shown in Fig. 3. The microstructures of longitudinal (*y*-plane) and cross-sections of the as-received extruded samples after solution annealing are shown in Fig. 3(a and c).The mean size of grains in transverse direction of the initial extruded rod was 50 µm ± 5. The microstructure presented in Fig. 3(b) shows a large numbers of copper-type or short shear bands on the longitudinal section after one pass of ECAP. These shear bands caused the fragmentation of the grains as shown in Fig. 3(d) on the cross-section (*x*-plane) view. This kind of shear bands has been reported by Duckham et al. [25] to be confined to one or a few adjacent grains. It should be mentioned that shear bands are a form of strain localization or plastic instability which can commonly be created under plane strain deformation conditions according to Dillamore et al. [26]. In addition, specimens having a supersaturated matrix are susceptible to natural aging and subsequent formation of GP zones as it has been reported by Zolotorevsky et al. [27]. These zones are in turn susceptible to shearing during ECAP process according to Chinh et al. [28]. Thus it can be concluded that for the solution annealed specimens, the presence of numerous shearable GP zone has aided the localization of the plastic deformation, hence formation of micro-shear bands. Referring to Miyamoto et al. [29] crystal orientation after one pass of ECAP processing on pure copper represented the main shear texture components was appeared in deformed sample and banded structure was formed by shear bands. Wang et al. [30] deformed an Al–Zn–Mg–Cu alloy having a strong initial texture by one pass of warm ECAP; he showed that shear occurs on two shear planes: the main shear plane where is close to the intersection plane of the two channels but with a small (5°) deviation and secondary shear plane which is perpendicular to the main shear plane.

A few mechanisms are reported about formation of shear bands. Referring to reports [31,32] the shear bands, originate due to the combination of shearable precipitates and very low or negative strain rate sensitivity. In age-hardenable aluminum alloys, formation of shearable precipitates resulting from dynamic strain aging (DSA) can cause strain localization and shear band formation [26,33] during tensile test. Huang et al. [34] have documented this

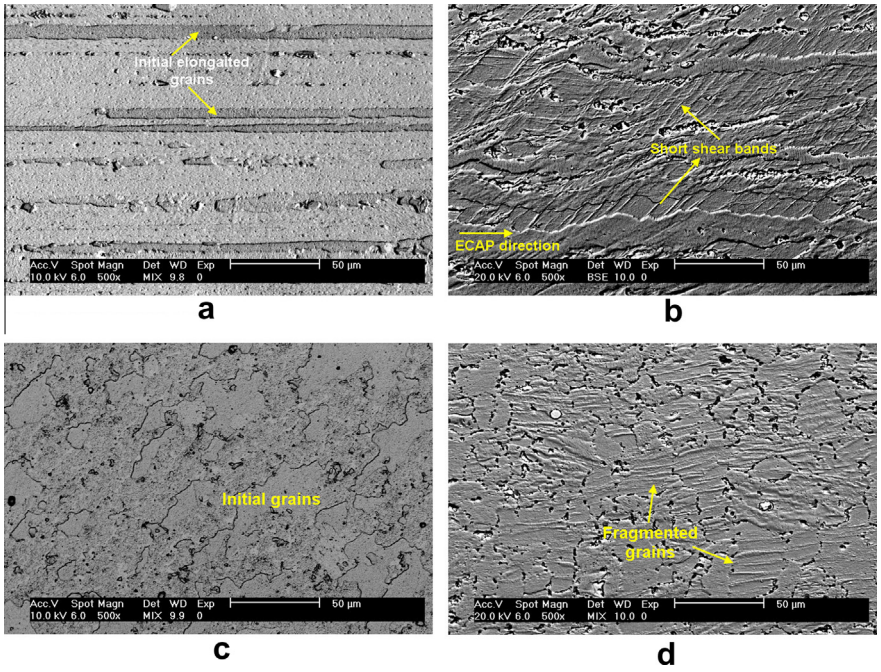

Fig. 3. Typical SEM micrograph of 2024 aluminum alloy microstructures, (a) solution annealed condition on longitudinal section, (b) after one pass of ECAP on longitudinal section, (c) solution annealed condition on cross-section, (d) after one pass of ECAP on cross-section.

behavior is supported by the ECAP process which is due to special die design can promote micro-shear banding. However referring to Chinh et al. [28] ECAP processing of Al–Zn–Mg–Cu alloy can cause the formation of micro-shear bands, may lead to catastrophic cracking or segmentation of the specimen at room temperature if dynamic strain aging is not controlled. The exact nature of the interaction between the precipitates and the dislocations was not established in this research but it seems that since the material used in this study was an age-hardenable aluminum alloy thereby formation of GP zone in solution annealed and water quenched sample has aided the formation of shear bands by strain localization during ECAP.

3.2. XRD analysis

XRD diagrams of solution annealed and deformed samples are illustrated in Fig. 4. For the solution annealed sample in order to minimize of initial texture effect the XRD data obtained from the longitudinal and transvers sections are presented in average in Fig. 4(a). These figures show reflections of planes in face centered cubic (FCC) structure. The diffraction peaks are broadened and their intensities are sharply decreased after one pass of ECAP at room temperature as shown in Fig. 4b. According to Ungar [35] this is due to an increases in lattice defects include linear and planar defects.

In order to analyze the peak broadening phenomenon, Rachinger's correction method [36] was used for separating $k\alpha1$ and $k\alpha2$ peaks in each diffraction peak of solution annealed sample. Then the average intensities in each peaks profile were plotted against diffraction vector $\boldsymbol{K = 2\mathrm{Sin}\,\theta/\lambda}$; where θ and λ are the Bragg's angle of the peak, and the wave length of Cu Kα, respectively. Experimental data were normalized to unity, and then fitted along with a pseudo-voigt function, which is the combination of Gaussian and Cauchy functions. The results obtained from diffraction of (111) and (200) lines are shown in Fig. 5. The scattering of diffraction data and peak broadening of the deformed sample is more than those of the solution annealed sample as shown in Fig. 5. According to Ungar [35] this can be due to an increase in linear defects specially dislocations formed during severe plastic deformation. Also the peaks shift which is shown in Fig. 5, express the ECAP process at room temperature cause a considerable amount of distortion in the lattice structure of the deformed materials, since according to Ungar [35] the peaks shift can be related to long range stresses as well as sub grain boundaries generated by deformation.

Modeling of the peak broadening is done, using mathematical relation between the structural full-width at half maximum height of the peak ($\Delta \boldsymbol{K_s}$) and average domain size (D) and the lattice micro-strain (ε) as given by Eq. (1), based on Williamson–Hall method [20];

$$\boldsymbol{\Delta K = \Delta K_s = 1/D + 2\varepsilon K} \quad (1)$$

The values of 2ε and D can be obtained from the slope and the ordinate intersection of the diagram of $\boldsymbol{\Delta K}$ vs. $\boldsymbol{K}$ respectively. The diagram obtained from three main diffraction lines of (111), (200) and (220) planes, is presented in Fig. 6. On the other hand, using Rietveld method [22], $\rho = (\rho_d \cdot \rho_s)^{1/2}$, the average dislocation density (ρ) can be estimated, where $\rho_d = 3/D^2$ (dislocation density due to the domain size effect) and $\rho_s = K\langle\varepsilon^2\rangle/b^2$ (dislocation density due to the lattice micro-strain), b is the Burger's vector and k is the material constant; equal 4 for 2024 aluminum alloy [37].

The structural parameters obtained from the X-ray diffraction analysis, are listed in Table 1. The domain size parameter of the solution sample (i.e. 588 nm) decreased to 107 nm after one pass of ECAP and the dislocation density of the solution sample (i.e. $6.18 \times 10^{12}\ \mathrm{m}^{-2}$) increased to $2.93 \times 10^{14}\ \mathrm{m}^{-2}$ after one pass of ECAP. This result is in accordance with results other works [9,38]. Zhao et al. [9] have documented that dislocation density of 7075 Al alloy calculated by XRD data analysis after two passes of ECAP increased to $9.4 \times 10^{14}\ \mathrm{m}^{-2}$. Also according to Gubizca et al. [38] research, dislocation density of an Al–Zn–Mg–Cu alloy after two passes of ECAP increased to $3.4 \times 10^{14}\ \mathrm{m}^{-2}$. Increase in dislocation density of 2024 Al alloy by a factor of about 50 times after one pass of ECAP in this study can sharply increase the yield

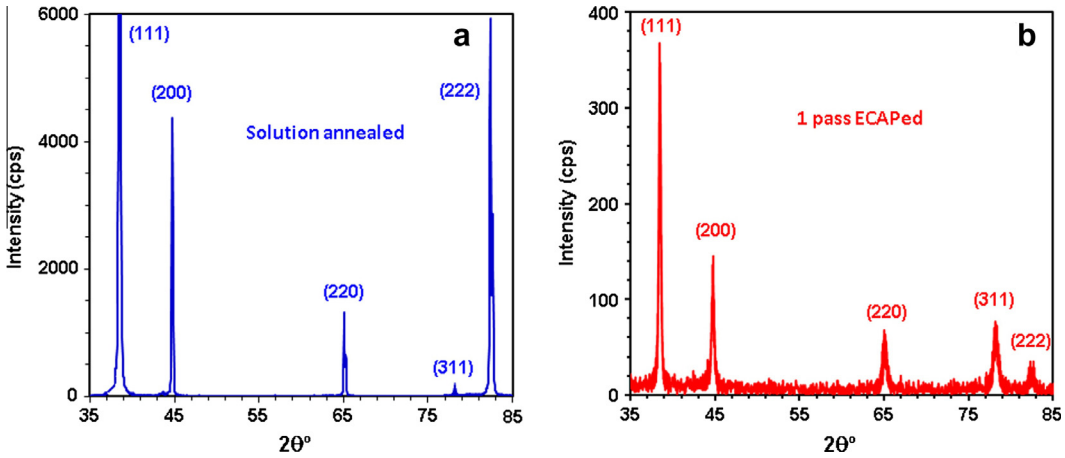

Fig. 4. XRD diagram of (a) the solution annealed 2024 Al alloy presented in average data obtained from the longitudinal and cross-sections and (b) the deformed sample by one pass of ECAP.

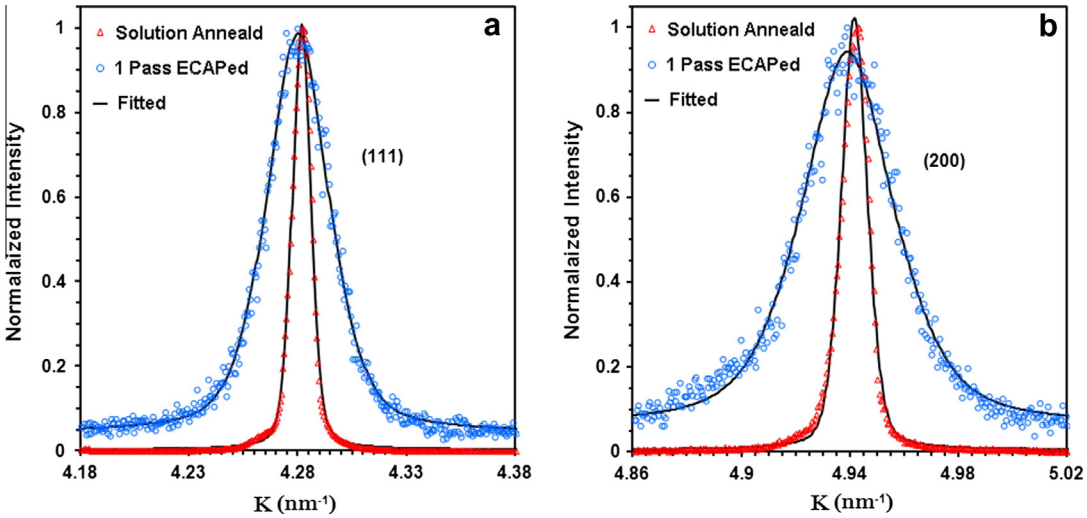

Fig. 5. Measured and fitted XRD peaks after normalizing vs. diffraction vector on the solution annealed and the deformed sample (a) (111) diffraction and (b) (200) diffraction.

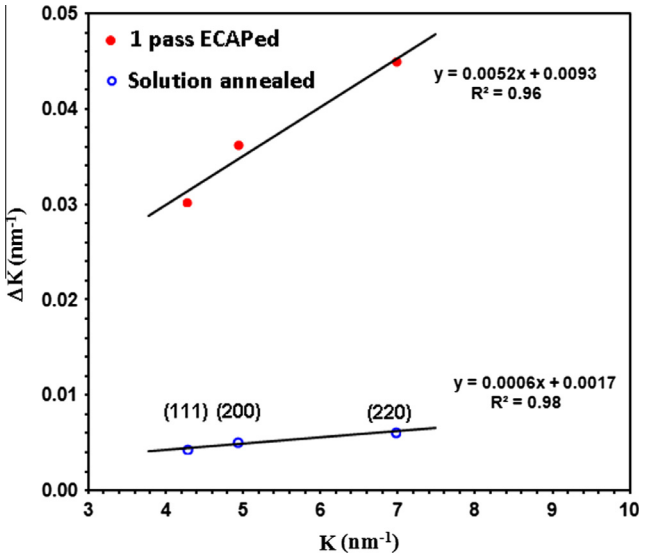

Fig. 6. Classic Williamson–Hall plot of the solution annealed 2024 Al alloy and the deformed sample by one pass of ECAP.

stress of the deformed material. Also As shown in Table 1 due to increase in dislocation density after deformation the dislocation spacing L is obviously decreased that it can be effective on the work hardening of the deformed sample.

3.3. Hardness measurement

The results of Vickers micro-hardness test using 1kgf load are shown in Fig. 7. This figure indicates that the mean micro-hardness of the sample T6, which aged at 100 °C after solution annealing, changed from 85 Hv_1 to 150 Hv_1 after 5 h of aging and then it became constant for further aging time. Mean micro-hardness of the deformed samples (labeled SE) increased from 85 Hv_1 to 170 Hv_1 immediately after one pass of ECAP. This sharp increase in micro-hardness can reflect a significant increase in dislocation density and their interaction with solute atoms during ECAP. One should pay attention that formation of a larger volume of precipitates is not possible at this short time, so the amount of increase observed in the hardness cannot be totally attributed to precipitation hardening.

According to Kim et al. [7] study, a large deformation energy can be generated in 6061 Al alloy during one pass of ECAP. This causes

Table 1
Structural parameters of the solution annealed and deformed 2024 aluminum alloys determined by X-ray diffraction peak analysis. D = domain size; $\langle\varepsilon\rangle$ = lattice microstrain; ρ_D = dislocation density due to lattice microstrain; ρ_S = dislocation density due to size effect; ρ = total dislocation density; L = dislocation spacing.

Sample	D(nm)	$\langle\varepsilon\rangle$ (%)	ρ_D (m^{-2})	ρ_S (m^{-2})	ρ (m^{-2})	L (nm) = $\rho^{-0.5}$
Solution annealed (S)	588	0.03	8.67E + 12	4.40E + 12	6.18E + 12	402
1 pass ECAPed (SE)	107	0.26	2.59E + 14	3.31E + 14	2.93E + 14	58

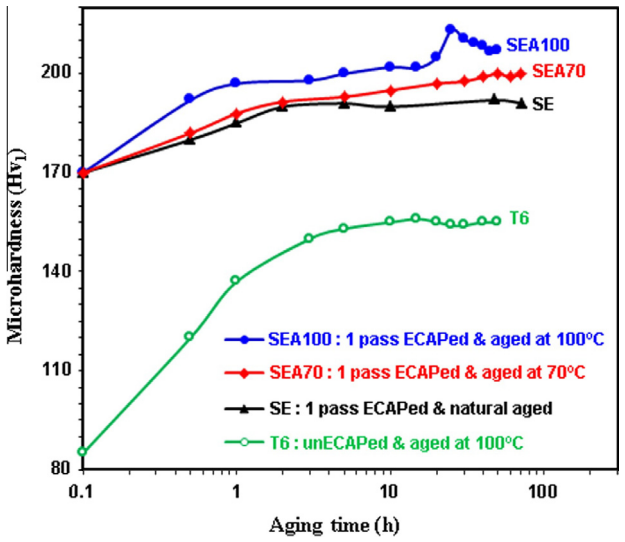

Fig. 7. Variation in hardness of 2024 Al alloy with and without ECAP as a function of aging time at different temperatures.

microstructural coarsening of the alloy during conventional aging at temperature range 170–190 °C. Consequently the hardness and yield stress of the alloy can be decreased. Therefore one may conclude from this discussion that aging of an aged hardenable Al alloys subjected to ECAP should be performed at temperatures lower than 170 °C in order to prevent grain growth. Aging at 100 °C was reported [7,8,10] as adequate temperature for precipitation hardening of age hardenable Al alloys after warm ECAP. In the present study, the samples aged at 100 °C after cold ECAP and for the first time aged at 70 °C to evaluate the effect of very low temperature aging on the mechanical properties of the ECAPed samples.

The mean hardness of the deformed sample (SE) increased from 170 Hv_1 to 190 Hv_1 during the first hour of natural aging, then it became constant for further aging time. Aging of the ECAPed sample at 70 °C (SEA70) caused an increase in micro-hardness up to 200 Hv_1 after 70 h, while aging at 100 °C for 25 h (SEA100) caused an increase in micro-hardness from 170 Hv_1 to 212 Hv_1, then it continued to decrease. This is in accordance with the results reported by Kim et al. [8] for aging of 2024 Al alloy at 100 °C after warm ECAP. Thus aging at 70 °C for 70 h is not only economical but also leads to lower hardness and strength when compared to the sample aged at 100 °C.

Increases in hardness during aging in 100 °C can be related to formation $CuMgAl_2$ phase. Referring to Zhao et al. [9], these precipitates can increase the hardness by retarding the dislocations movement within the microstructure by forcing dislocations to either cut across or encircle the fine precipitates.

3.4. Tensile properties

Engineering stress–strain curves obtained for various samples are shown in Fig. 8. According to May et al. [39] corrugated flow stress curves are due to dynamic strain aging. That means trapping of dislocations by precipitates or impurity atoms lead to serration of the flow curve. The exact data obtained from the flow curves i.e. yield stress (YS) and ultimate tensile stress (UTS) and the amount of elongation to failure of the specimens are presented in Table 2. Significant increase in YS was obtained after one pass of ECAP deformation. The yield strength of the sample at solution condition (i.e. 185 MPa) increased after one pass of cold ECAP and natural aging for 72 h to 575 MPa; this means an increase of 210%. This amount of increase in yield strength is much higher than those obtained for other tempered 2024 Al alloy including T4, T6 and even T8. The yield stress of the sample after one pass of ECAP was more than those of T4, T6 and T8 by about 50%, 40% and 20% respectively. However one should note that the amount of elongation of the solution sample decreased from 18.5% to 7.2% after one pass of cold ECAP. This means a 60% reduction in elongation due to ECAP at room temperature.

A sharp increase in yield strength after one pass of ECAP indicates the severity of deformation and remarkable changes in the microstructure especially increase in dislocations density during ECAP as presented in Table 1. The decline in ductility can be due to the presence of the shear bands within the microstructure. According to Csontos and Starke [32], these shear bands can increase the intensity of planar slip trespassing on a grain boundary, thereby encouraging low-energy inter-granular fracture surface and low ductility during tensile test.

Aging of the deformed sample at 70 °C increased its strength slightly. This is an indication that the stored energy induced by one pass of ECAP was not enough to help the kinetic of precipitates transformations at this temperature. The higher yield stress (i.e. 610 MPa) and tensile strength (i.e. 670 MPa) were obtained for the sample aged at 100 °C for 25 h. This result is consistent with those reported by Kim et al. [8] who applied severe plastic deformation (SPD) on 2024-T351 Al alloy by one pass of ECAP at

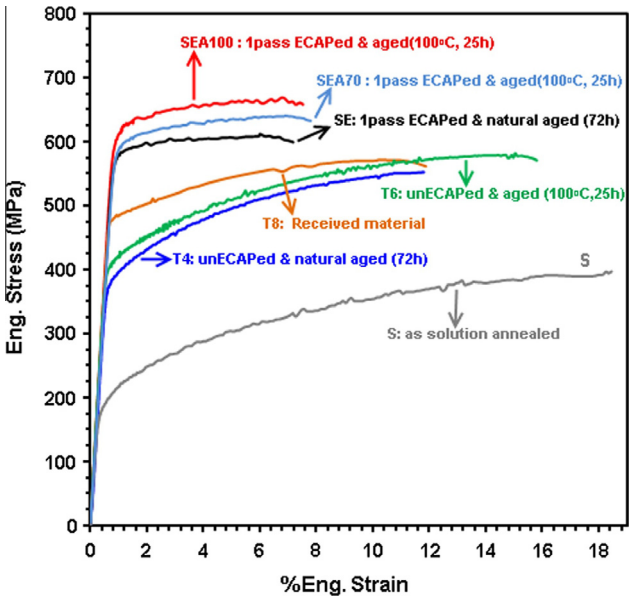

Fig. 8. Tensile stress–strain curves for various samples before and after ECAP and aged at different temperatures.

Table 2
Tensile properties of 2024 Al alloy before and after one pass of ECAP.

Sample	Process	YS (MPa)	UTS(MPa)	Elongation to failure (%)	Strain hardening component (n)
S	Solution + water quench	185	393	18.5	0.281
T4	WQ + natural aging (72 h)	385	552	11.8	0.192
T6	WQ + aging (100 °C,25 h)	414	578	15.8	0.181
T8	As-received material	485	574	11.9	0.117
SE	WQ + 1pass ECAP + Natural aging (72 h)	575	608	7.5	0.053
SEA70	WQ + 1pass ECAP + Aging (70 °C,70 h)	595	647	7.8	0.069
SEA100	WQ + 1pass ECAP + Aging (100 °C,25 h)	610	670	7.7	0.069

160 °C. Application of warm ECAP can reduce dislocations density due to dynamic recovery during SPD because referring to Kim et al. [40] softening mechanism by cross slip makes a significant contribution to the softening of 7075 aluminum alloy during warm ECAP. Consequently this reduction of dislocations density can lead to an increase in the potential of material to be work hardened further during tensile test. However using cold ECAP, caused the formation of higher dislocations density, so that the rate of work hardening reduced, hence lower UST (670 MPa) obtained during tensile test, in comparison to that obtained by Kim et al. (i.e. 715 MPa). Meanwhile it should be mentioned that the initial material used in this study (i.e. 2024-T8 Al alloy) had more hardness than the 2024-T351 Al alloy used by Kim et al. [8] in their work. Also one should notice that the presence of shear bands within the microstructure of ECAPed sample can specially lead to less amount of ductility during tensile test.

In order to evaluate the change in work hardening of the specimens, the strain hardening exponents (n) were calculated by measuring the slopes of the curves presented in Fig. 9. The calculated values of n are summarized in Table 2.

Considerable work hardening occurred during tensile test in the unreformed samples which includes samples in solution condition, T4 and T6 tempered as shown in "n", values in Table 2. This suggests that initial dislocation density within the microstructures of the samples was low, so during tensile test generation of a large number of dislocations was possible. These dislocations interacted with one another and also with the precipitates; led to more strength and hardness of the samples. On the other hand due to high formation of dislocation during ECAP at room temperature, the spacing between dislocations reduced as shown in Table 1, led to reduction in work hardening rate during tensile test, so that the slope of the curve related to sample SE became flattened as shown in Fig. 8.

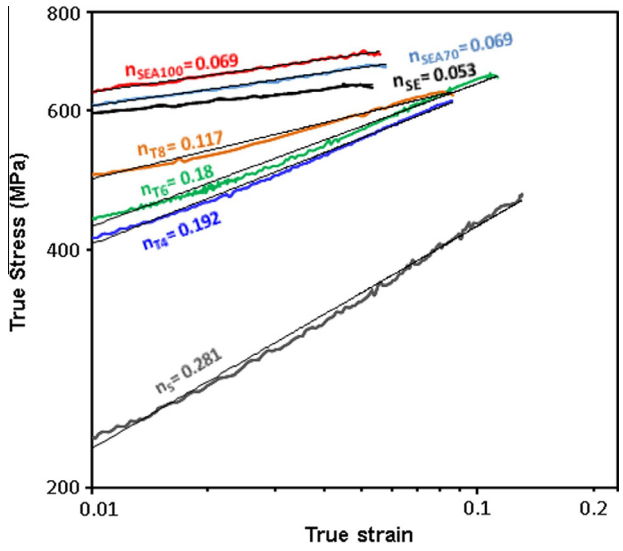

Fig. 9. The true stress–strain curves of the various samples after yield points.

Aging of the deformed sample at 70 °C and 100 °C increased the strain hardening exponent (n) slightly. Increase in exponent "n", in a similar work by Kim et al. [41] on the ECAP of 6061 Al alloy has been attributed to: 1 – decrease of solutes atoms in solid solution; 2 – formation of precipitates and 3 – reduction in dislocations density. However since in the present study reduction in dislocation density is limited during aging due to widespread presence of shear bands within the microstructure, strain hardening exponent of the deformed and aged specimens (i.e. SEA70 and SEA100) can slightly increase during subsequent aging due to the above mentioned factors 1 and 2, as shown in Fig. 9 and Table 2.

According to Zhao et al. [9], increasing the dislocations density is the main mechanism of hardening in 7075 aluminum alloy subjected to warm ECAP. In this study as shown in Table 2 the increase in yield stress occurred in the sample subjected to SPD i.e. sample SE, is much more than those of the samples which merely subjected to aging cycles i.e. T4 and T6. Therefore, one may conclude that the main factors of strengthening for the deformed sample were initially an increase in dislocations density, then their interaction with one another and with solute atoms during ECAP. However formation of shear bands during ECAP had significant effect on the ductility of the deformed materials during tensile test.

4. Conclusions

1. Severe plastic deformation of 2024 aluminum alloy with one pass of ECAP at room temperature generated copper-type or short shear bands within the microstructure.
2. The result of X-ray diffraction analysis showed that the dislocation density of the solution annealed sample considerably increased and dislocation spacing decreased after one pass of cold ECAP processing.
3. Significant increases in hardness and yield strength of the deformed and aged material can be attributed to increase in dislocation density and their interaction with one another and with solute atoms during ECAP.
4. Aging at 70 °C after deformation slightly increased the hardness and yield stress of the deformed material, but aging in 100 °C relatively improved these properties due to precipitation hardening although had no effect on the ductility.

References

[1] R.Z. Valiev, R.K. Islamgaliev, I.V. Alexandrov, Progress in Materials Science 45 (2000) 103–189.
[2] R.Z. Valiev, T.G. Langdon, Progress in Materials Science 51 (2006) 881–981.
[3] V. Segal, V. Reznikov, A. Drobyshevskii, V. Kopylov, Metally 1 (1981) 115–123.
[4] Z. Horita, T. Fujinami, T.G. Langdon, Materials Science and Engineering: A 318 (2001) 34–41.
[5] P. Chaudhury, B. Cherukuri, R. Srinivasan, Materials Science and Engineering: A 410 (2005) 316–318.
[6] Z. Horita, T. Fujinami, M. Nemoto, T. Langdon, Journal of Materials Processing Technology 117 (2001) 288–292.

[7] W. Kim, J. Kim, T. Park, S. Hong, D. Kim, Y. Kim, J. Lee, Metallurgical and Materials Transactions A 33 (2002) 3155–3164.
[8] W. Kim, C. Chung, D. Ma, S. Hong, H. Kim, Scripta Materialia 49 (2003) 333–338.
[9] Y. Zhao, X. Liao, Z. Jin, R. Valiev, Y. Zhu, Acta Materialia 52 (2004) 4589–4599.
[10] W. Kim, J. Wang, Materials Science and Engineering: A 464 (2007) 23–27.
[11] C. Cepeda-Jiménez, J. García-Infanta, O.A. Ruano, F. Carreño, Journal of Alloys and Compounds 509 (2011) 8649–8656.
[12] T. Kvackaj, R. Bidulsky, Aluminum Alloys, Theory and Applications, InTech, Rijeka, 2011.
[13] T. Kvačkaj, J. Bidulská, M. Fujda, R. Kočiško, I. Pokorný, O. Milkovic, Materials Science Forum 633–634 (2010) 273–302.
[14] E.A. El-Danaf, Materials & Design 32 (1050) (2011) 3838–3853.
[15] S.G. Chowdhury, A. Mondal, J. Gubicza, G. Krállics, A. Fodor, Materials Science and Engineering: A 490 (2008) 335–342.
[16] J. Bidulská, T. Kvackaj, R. Bidulský, M. Actis Grande, Acta Physica Polonica A 122 (2012) 553–556.
[17] Y. Iwahashi, Z. Horita, M. Nemoto, J. Wang, T.G. Langdon, Scripta Materialia 35 (1996) 143–146.
[18] M. Furukawa, Y. Iwahashi, Z. Horita, M. Nemoto, T.G. Langdon, Materials Science and Engineering: A 257 (1998) 328–332.
[19] B.E. Warren, X-ray Diffraction, Courier Dover Publications, 1969.
[20] G. Williamson, W. Hall, Acta Metallurgica 1 (1953) 22–31.
[21] T. Ungár, I. Dragomir, Á. Révész, A. Borbély, Journal of Applied Crystallography 32 (1999) 992–1002.
[22] P. Mukherjee, A. Sarkar, P. Barat, S. Bandyopadhyay, P. Sen, S. Chattopadhyay, P. Chatterjee, S. Chatterjee, M. Mitra, Acta Materialia 52 (2004) 5687–5696.
[23] E. Starke, Materials Science & Engineering 29 (1977) 99–115.
[24] Z. Huda, N.I. Taib, T. Zaharinie, Materials Chemistry and Physics 113 (2009) 515–517.
[25] A. Duckham, R. Knutsen, O. Engler, Acta Materialia 49 (2001) 2739–2749.
[26] I. Dillamore, J. Roberts, A. Bush, Metal Science 13 (1979) 73–77.
[27] N.Y. Zolotorevsky, A. Solonin, A.Y. Churyumov, V. Zolotorevsky, Materials Science and Engineering: A 502 (2009) 111–117.
[28] N.Q. Chinh, J. Gubicza, T. Czeppe, J. Lendvai, C. Xu, R.Z. Valiev, T.G. Langdon, Materials Science and Engineering: A 516 (2009) 248–252.
[29] H. Miyamoto, J. Fushimi, T. Mimaki, A. Vinogradov, S. Hashimoto, Materials Science and Engineering: A 405 (2005) 221–232.
[30] S.C. Wang, M.J. Starink, N. Gao, X.G. Qiao, C. Xu, T.G. Langdon, Acta Materialia 56 (2008) 3800–3809.
[31] D. Dumont, A. Deschamps, Y. Brechet, Materials Science and Engineering: A 356 (2003) 326–336.
[32] A.A. Csontos, E.A. Starke, International Journal of Plasticity 21 (2005) 1097–1118.
[33] M. Roshan, S. Jahromi, R. Ebrahimi, Journal of Alloys and Compounds 509 (2011) 7833–7839.
[34] Y. Huang, J. Robson, P. Prangnell, Acta Materialia 58 (2010) 1643–1657.
[35] T. Ungar, Scripta Materialia 51 (2004) 777–781.
[36] W.A. Rachinger, Journal of Scientific Instruments 25 (1948) 254.
[37] K. Bendo Demetrio, Cryomilling and Spark Plasma Sintering of 2024 Aluminium Alloy, in: University of Trento, 2011.
[38] J. Gubicza, I. Schiller, N. Chinh, J. Illy, Z. Horita, T. Langdon, Materials Science and Engineering: A 460 (2007) 77–85.
[39] J. May, H. Höppel, M. Göken, Scripta Materialia 53 (2005) 189–194.
[40] W. Kim, J. Kim, H. Kim, J. Park, Y. Jeong, Journal of Alloys and Compounds 450 (2008) 222–228.
[41] J. Kim, H. Kim, J. Park, W. Kim, Scripta Materialia 53 (2005) 1207–1211.